Virologica Sinica 38 (2023) 96–107

Contents lists available at ScienceDirect

Virologica Sinica

journal homepage: www.keaipublishing.com/en/journals/virologica-sinica
www.virosin.org

Research Article

OGG1 inhibition suppresses African swine fever virus replication

Jie Fan [a,b], Xinqian Lv [b], Saixia Yang [b], Shuxian Geng [a,b], Jifei Yang [b], Yaru Zhao [b], Zhonghui Zhang [b], Zhijie Liu [b], Guiquan Guan [b], Jianxun Luo [b], Qiaoying Zeng [a,*], Hong Yin [b,c], Qingli Niu [b,*]

[a] College of Veterinary Medicine, Gansu Agricultural University, Lanzhou, 730070, China
[b] African Swine Fever Regional Laboratory of China (Lanzhou), State Key Laboratory of Veterinary Etiological Biology, Key Laboratory of Veterinary Parasitology of Gansu Province, Lanzhou Veterinary Research Institute, Chinese Academy of Agricultural Sciences, Lanzhou, 730046, China
[c] Jiangsu Co-Innovation Center for the Prevention and Control of Important Animal Infectious Disease and Zoonosis, Yangzhou University, Yangzhou, 225009, China

ARTICLE INFO

Keywords:
African swine fever virus (ASFV)
8-oxoguanine DNA glycosylase 1 (OGG1)
8-oxo-7,8-dihydroguanine (8-oxoG)
Inhibitors
Antiviral effect

ABSTRACT

African swine fever virus (ASFV) is an important pathogen that causes a highly contagious and lethal disease in swine, for which neither a vaccine nor treatment is available. The DNA repair enzyme 8-oxoguanine DNA glycosylase 1 (OGG1), which excises the oxidative base lesion 8-oxo-7,8-dihydroguanine (8-oxoG), has been linked to the pathogenesis of different diseases associated with viral infections. However, the role of OGG1-base excision repair (BER) in ASFV infection has been poorly investigated. Our study aimed to characterize the alteration of host reactive oxygen species (ROS) and OGG1 and to analyse the role of OGG1 in ASFV infection. We found that ASFV infection induced high levels and dynamic changes in ROS and 8-oxoG and consistently increased the expression of OGG1. Viral yield, transcription level, and protein synthesis were reduced in ASFV-infected primary alveolar macrophages (PAMs) treated by TH5487 or SU0268 inhibiting OGG1. The expression of BER pathway associated proteins of ASFV was also suppressed in OGG1-inhibited PAMs. Furthermore, OGG1 was found to negatively regulate interferon β (IFN-β) production during ASFV infection and IFN-β could be activated by OGG1 inhibition with TH5487 and SU0268, which blocked OGG1 binding to 8-oxoG. Additionally, the interaction of OGG1 with viral MGF360-14-L protein could disturb IFN-β production to further affect ASFV replication. These results suggest that OGG1 plays the crucial role in successful viral infection and OGG1 inhibitors SU0268 or TH5487 could be used as antiviral agents for ASFV infection.

1. Introduction

African swine fever virus (ASFV), as a contagious viral pathogen, is responsible for a rapid spread and highly lethal disease characterized by fever, haemorrhage, ataxia, and severe depression among domestic pigs that poses serious economic consequences to the swine industry and international trade (Cackett et al., 2020). More recently, in 2018, ASFV was introduced into China and spread rapidly through many provinces, presenting a severe threat to the pork supply (Zhou et al., 2018). Despite its importance, little is known regarding the mechanisms and regulation of ASFV infection.

Early expression of proteins of most viruses is not only important to virus survival but also changes the cell environment of the host, such as elevating cell reactive oxygen species (ROS) levels and causing DNA oxidative damage, which is an important innate immune defence of the host against viral infection (Cardoso et al., 2016). DNA bases are susceptible to ROS, especially guanine, and its oxidation product 7,8-dihydro-8-oxoguanine (8-oxoG) is the most notable endogenous base lesion in DNA, often used as a cellular biomarker to indicate oxidative stress (Wang W. et al., 2021). 8-oxoG can pair with adenine as well as cytosine, thereby causing G to T transversion mutations during DNA replication, which is considered to play a role in mutagenesis and carcinogenesis (Shibutani et al., 1991). To counteract these undesirable biological effects, the DNA damage response (DDR) has specifically evolved to sense damage sites and activate an arsenal of enzymes for DNA damage repair. Base excision repair (BER) is one type of the pivotal DDR used to repair the oxidative DNA damage (Anand et al., 2020). Beyond its canonical role in mediating DNA repair, the DDR also functions as a potent antiviral defence in host cells (Weitzman et al., 2010). However, viruses always take advantage of the DDR pathways to modulate the chromatin epigenetic signatures and hijack cellular proteins to support viral replication (Verhalen et al., 2015). A

* Corresponding authors.
E-mail addresses: zengqy@gsau.edu.cn (Q. Zeng), niuqingli@caas.cn (Q. Niu).

https://doi.org/10.1016/j.virs.2022.11.006
Received 21 June 2022; Accepted 18 November 2022
Available online 23 November 2022

previous study indicated that the ATR-mediated DNA single-strand break repair pathway facilitated ASFV infection (Simoes et al., 2013). It is not yet clear whether the induction of oxidative damage results from successful ASFV infection, and no studies have been performed to evaluate the role of BER in viral replication.

Many nucleocytoplasmic large DNA virus (NCLDV)-encoded proteins may take part in viral DNA damage repair pathways. ASFV is a large DNA virus belonging to the *Asfarviridae* family and *Asfivirus* genus that primarily replicates in the cytoplasm of swine macrophage cells, which are rich in free oxygen radicals (Cuesta-Geijo et al., 2022). Intriguingly, ASFV evolved its own BER system to overcome genome damage, including an apurinic/apyrimidinic (AP) endonuclease (AsfvAP, E296R) (Chen et al., 2020), a ligase (AsfvLIG, NP419 L) (Lamarche et al., 2005), and a polymerase (AsfvPolX, O174 L) (Jezewska et al., 2006). In cellular organisms, BER is initiated by DNA glycosylase, further recognizing specific base damage and removing it. In mammals, 8-oxoguanine DNA glycosylase 1 (OGG1), which is the major DNA glycosylase located in both the nucleus and mitochondria, repairs DNA damage by recognizing 8-oxoG and cleaving the glycosidic bond, removing the 8-oxoG and generating an AP site in the DNA, further inducing the downstream pathway of BER (Nakabeppu et al., 2004; Wang K. et al., 2021). OGG1 is a multifunctional protein that not only acts as a glycosidase initiating BER but also participates in epigenetic regulation in gene transcription (Wang et al., 2018). The loss or functional deficiency of OGG1 is relevant in many pathological conditions, including cancer, inflammation, and neurodegenerative diseases (Pao et al., 2020; Visnes et al., 2018, 2020). It has been demonstrated that virus-induced oxidative stress and triggered DNA damage repair responses in infected cells are closely related to pathogenesis, and OGG1 is pivotal for the successful infection of a variety of viruses (Hu et al., 2011; Piciocchi et al., 2016; Schachtele et al., 2010). However, as ASFV does not encode genes of OGG1-like glycosylase, it is possible that the virus uses the cellular enzyme to switch on the ASFV-BER system and regulate related biological processes (Alejo et al., 2018).

In the present study, we examined the induction of ROS resulting from ASFV infection and evaluated its effects on the host DNA damage and repair machinery. Furthermore, we evaluated the biological function of OGG1 and its inhibitory effect on the replication and transcription of ASFV *in vitro*. The results suggested that the tested OGG1 inhibitors TH5487 and SU0268 were able to effectively inhibit ASFV infection and might be used potentially as the preventative antiviral drugs.

2. Materials and methods

2.1. Field samples collection, cells culture and ASFV strain

Healthy lungs and clinical lungs infected with ASFV were collected as described previously (Sun et al., 2021). Primary alveolar macrophages (PAMs) were obtained from 40- to 60-day-old SPF pigs as previously described (MALMQUIST and HAY, 1960). PAM and MA104 cells were incubated in RPMI 1640 medium (0013219, BI, Israel)) containing 10% fetal bovine serum (10091148, Gibco, USA) and 1% penicillin-streptomycin (V900929, Sigma, USA) at 37 °C in a humidified incubator with 5% CO_2. Red blood cells from heparin sodium-treated swine blood were washed twice with PBS (P1020, Solarbio, China), kept in RPMI 1640 medium containing 1% penicillin-streptomycin solution, and maintained at 4 °C for the haemadsorption (HAD) assay. The genotype II ASFV strain (CN/SC/2019) was provided by African Swine Fever Regional Laboratory of China (Lanzhou).

2.2. Antibodies and reagents

The antibodies used in this study are as follows: rabbit polyclonal anti-OGG1 (15125-1-AP), rabbit polyclonal anti-GAPDH (10494-1-AP), Flag-tag monoclonal antibody (66008-4-Ig), HA-tag monoclonal antibody (66006-2-Ig) and horseradish peroxidase (HRP)-conjugated goat anti-rabbit or anti-mouse secondary antibodies (SA00001-2; SA00013-3) were obtained from Protein Tech Group, China. Monoclonal antibody 8-oxoG (sc-130,914) was purchased from Santa Cruz Biotechnology, USA. β-tubulin monoclonal antibody (32-2600), goat anti-rabbit IgG (H+L) (Alexa Fluor 488, A32731) and goat anti-mouse IgG (H+L) secondary antibodies (Alexa Fluor 555, A28180) were purchased from Invitrogen, USA. Anti-p30, anti-p72, anti-pO174 L, anti-pE296R and anti-pNP419 rabbit polyclonal antibodies were provided by the African Swine Fever Regional Laboratory, China (Lanzhou), Lanzhou Veterinary Research Institute (LVRI) of the Chinese Academy of Agricultural Sciences. SU0268 was synthesized as previously described (Tahara et al., 2018). TH5487 (6749) was purchased from Tocris Bioscience, UK. Dimethyl sulfoxide (DMSO) was purchased from Sigma-Aldrich, USA.

2.3. Cytotoxicity assay

The cell cytotoxicity of two representative inhibitors was evaluated in PAMs by using a CCK8 Kit (Cat K1018, APExBIO, USA). Briefly, PAMs (2×10^4 cells per well) in 96-well cell culture plates were treated with increasing concentrations of inhibitors. The experiments included three replicates, and a blank and DMSO control were included. The treated cells were incubated for 24 h at 37 °C in 5% CO_2, and after incubation, 10 μL CCK8 was added in each well and incubated at 37 °C for 1–4 h. The absorbance was measured using a microplate reader at wavelength of 450 nm (OD_{450}). The cell viability of PAMs was calculated according to the formula: cell viability rate (%) = [(OD inhibitor − OD blank)/(OD control − OD blank)] × 100%. The drug concentration leading to 50% cytopathic (CC_{50}) was calculated using GraphPad Prism 8.0 software (GraphPad, Inc., La Jolla, CA, USA).

2.4. Genomic DNA extraction and 8-oxoG measurement

PAMs were harvested and rinsed twice with PBS. Then, genomic DNA from cells were extracted using a Blood & Cell Culture DNA Mini Kit (13323, Qiagen, Germany). Genomic DNA from tissues was isolated using a QIAamp DNA Mini Kit (56304, Qiagen) according to the manufacturer's instructions. The level of 8-oxoG was assessed by using a commercial ELISA kit (4661, Chemicalbook, China) according to the manufacturer's instructions. Meanwhile, the absorbance was immediately read at wavelength of 450 nm by a microplate reader (ThermoFisher Scientific, USA).

2.5. Analysis of oxidized glutathione (GSH) disulfide (GSSG) concentration

The PAMs were lysed with 5% 5-sulfosalicylic acid solution. The cellular level of GSSG was determined using a Glutathione Oxidized (GSSG) Colorimetric Assay Kit (GC31353, Glpbio, USA) following the manufacturer's protocol. The absorption values were measured at wavelength of 485 nm and 528 nm by a microplate reader.

2.6. HAD_{50} assay

Primary PAMs were seeded in 96-well plates. The samples were then added to the plates and titrated in triplicate using 10× dilutions. The presence of ASFV was assessed by identification of the characteristic rosette formation representing HAD of erythrocytes around the infected cells. HAD was observed for 7 days, and the 50% HAD (HAD_{50}) was calculated by using the method of Reed and Muench (Ruiz-Gonzalvo et al., 1996).

2.7. Reverse transcription-quantitative PCR

Total RNA was extracted from cultured PAMs using TRIzol reagent (15596018, Invitrogen) according to the manufacturer's instructions. qRT-PCR was performed with a Step Prime Script RT PCR Kit (RR064A,

Takara, Japan). The PCR primer sequences used in the reaction are listed in Supplementary Table S1. The relative expression of each designated gene was calculated by the $2^{-\triangle\triangle Ct}$ method and normalized to *GAPDH* (*$P < 0.05$, Student's *t*-test).

2.8. Western blot analysis

PAMs were lysed in 200 μL RIPA lysis buffer (89900, ThermoFisher Scientific, USA) with protease inhibitor cocktail (78429, ThermoFisher Scientific, USA) for 30 min on ice. After centrifugation, the lysates were denatured for 10 min in 2× SDS-PAGE loading buffer (S3401, Sigma Aldrich). Samples were separated by electrophoresis on SDS-PAGE gels and then transferred to transfer nitrocellulose membranes (ISEQ00010, Merck-Millipore, USA). Next, membranes were blocked with 5% skimmed milk for 1 h at room temperature. After that, the membranes were incubated with primary antibodies at 4 °C overnight, and then incubated with corresponding secondary antibodies conjugated to HRP at room temperature for 1 h. Finally, the relative expression levels of protein were detected using ECL reagents (35055, ThermoFisher Scientific) and were quantified by Quantity One software (Bio-Rad Laboratories, USA).

2.9. Immunofluorescence and confocal microscopy

PAMs were seeded in laser confocal plates, treated under different conditions and then washed twice with PBS. Then, monolayers were fixed using 4% paraformaldehyde (R37814, ThermoFisher Scientific) for 30 min and permeabilized with 0.1% Triton-X 100 (X100, Sigma-Aldrich) for 20 min at room temperature. Next, the cells were blocked with 5% BSA (SRE0096, Sigma Aldrich) for 1 h at room temperature. Then, the cells were incubated with primary antibodies at 4 °C overnight and then incubated with fluorochrome-conjugated secondary antibodies for 1 h in the dark. Meanwhile, the cells were incubated with DAPI (P36941, Invitrogen) for nuclear staining. Finally, the fluorescence signals were detected with a TCS SP8 confocal fluorescence microscope (Leica, Germany).

2.10. siRNA assay and plasmids transfection

Two double-stranded siRNAs targeting OGG1 transcripts were designed by Ribobio, China. The siRNA sequences used in the study are shown in Supplementary Table S1. For knockdown of OGG1, siRNA control or siRNA-OGG1 was transfected into PAMs using Lipofectamine 2000 (R0532, Invitrogen). After 24 h of incubation, the knockdown efficiency of target gene was validated by qRT-PCR and Western blot.

The Flag-MGF360-14-L and HA-OGG1 expression plasmids were constructed by Sangon Biotech, China. The recombinant plasmids were transfected into cells with Lipofectamine 2000 when the MA104 cells had grown to nearly 80% confluence. Then, 24 h after transfection, cells were harvested and analyzed by different methodologies.

2.11. Co-immunoprecipitation (Co-IP) assay

The MA104 cells were co-transfected with the indicated plasmids. The transfected cells were lysed and clarified by centrifugation at 160 ×*g* at 4 °C for 15 min. The supernatants were incubated with anti-Flag or anti-HA antibodies and rotated at 4 °C overnight. Protein G magnetic beads (10004D, Invitrogen) were added to each sample and incubated at 4 °C for 2 h. Immunocomplex was recovered by adsorption and gently washed six times with lysis buffer, and eluted by boiling in sample buffer, then subjected to immunoblotting to evaluate the relationship between proteins.

2.12. Co-IP-mass spectrometry (MS)

Firstly, PAMs were infected with ASFV for 48 h, then, the whole cell extracts were immunoprecipitated by OGG1 antibody or IgG control. Secondly, the IP protein samples were subjected to SDS-polyacrylamide gel electrophoresis, stained with Coomassie blue, and detected by mass spectrometry in Sangon Biotech.

2.13. Statistical analysis

Statistical analysis of all data was performed using Prism 8.0 (GraphPad Software, Inc., USA). Two-tailed *P* values were assessed, and *P* values < 0.05 were considered to be statistically significant (*$P < 0.05$; **$P < 0.01$, ***$P < 0.001$ and ****$P < 0.0001$). Statistical comparisons between groups were performed using paired or non-paired *t*-tests. The CC_{50} was calculated by a linear regression analysis of dose-response curves generated from the obtained data. The 95% confidence intervals (95% CIs) for CC_{50} were calculated using IBM SPSS Statistics version 19.0, USA. Quantitative data displayed in all figures are expressed as the means ± standard devision (SD, represented as error bars).

3. Results

3.1. ASFV infection induced dynamic changes in ROS and promoted 8-oxoG production

GSH is a tri-peptide (γ-glutamyl-L-cysteinylglycine) that acts as a free radical scavenger and protects cells from oxidative stress, and it can be oxidized by cellular ROS, forming GSSG. The concentration of GSSG is an indicator of ROS levels (Owen and Butterfield, 2010). Therefore, GSSG production was detected to reflect the level of ROS post-ASFV infection. ROS can produce numerous DNA base modifications, especially causing 8-oxoG lesions. Here, we also examined 8-oxoG, which is a marker of DNA base oxidation in ROS-induced DNA damage. To mimic oxidative stress, H_2O_2 was used as a positive control. ROS and 8-oxoG production during ASFV infection were detected by using a Glutathione Oxidized (GSSG) Colorimetric Assay Kit and ELISA, and the results indicated that ROS and 8-oxoG were elicited from ASFV-infected PAMs at 0.25 h post-infection (hpi), and showed dynamic changes later (Fig. 1A and B). The production of ROS in ASFV-infected cells increased from 0.25 hpi to 3 hpi, followed by a decrease, where the ROS level was reduced to approximately equal to that in the mock group at 9 hpi, and then rebounded to its peak at 12 hpi (Fig. 1A). In addition, the formation of 8-oxoG was measured by ELISA using an 8-oxoG-specific antibody in ASFV-positive or -negative tissues. Similar to cell infection, a high amount of 8-oxoG was observed in the ASFV-infected lungs compared to healthy lungs (Fig. 1B and C). Meanwhile, immunofluorescence results also showed a strong accumulation of 8-oxoG at 1 hpi in ASFV infected-PAMs (Fig. 1D). These results indicated that ROS and the oxidized DNA base 8-oxoG were produced during ASFV infection, suggesting the involvement of ROS in virus-induced DNA lesions.

3.2. The DNA repair enzyme OGG1 was elicited in ASFV-infected PAMs with dynamic expression

To investigate the effects of ROS-induced DNA oxidative damage repair during ASFV infection, we analyzed the expression of the lesion-specific BER enzyme OGG1. Initially, to rule out the potential influence of cell activity which may result from ASFV infection, we observed the cytopathic effect (CPE) and measured cell activity at different time points after ASFV infection. ASFV replicated and proliferated in PAMs but did not cause CPE under general conditions (Supplementary Fig. S1A). Moreover, cell viability was detected by using the CCK-8 assay to determine whether ASFV infection can influence cell survival compared with normal and H_2O_2-stimulated cells. The results indicated that cell viability was not significantly reduced after H_2O_2 treatment or ASFV infection until at least 24 hpi, and the cell survival rate was still approximately 50% at 48 hpi (Supplementary Fig. S1B). The transcriptional level of OGG1 was increased over time in H_2O_2-treated or AFSV-

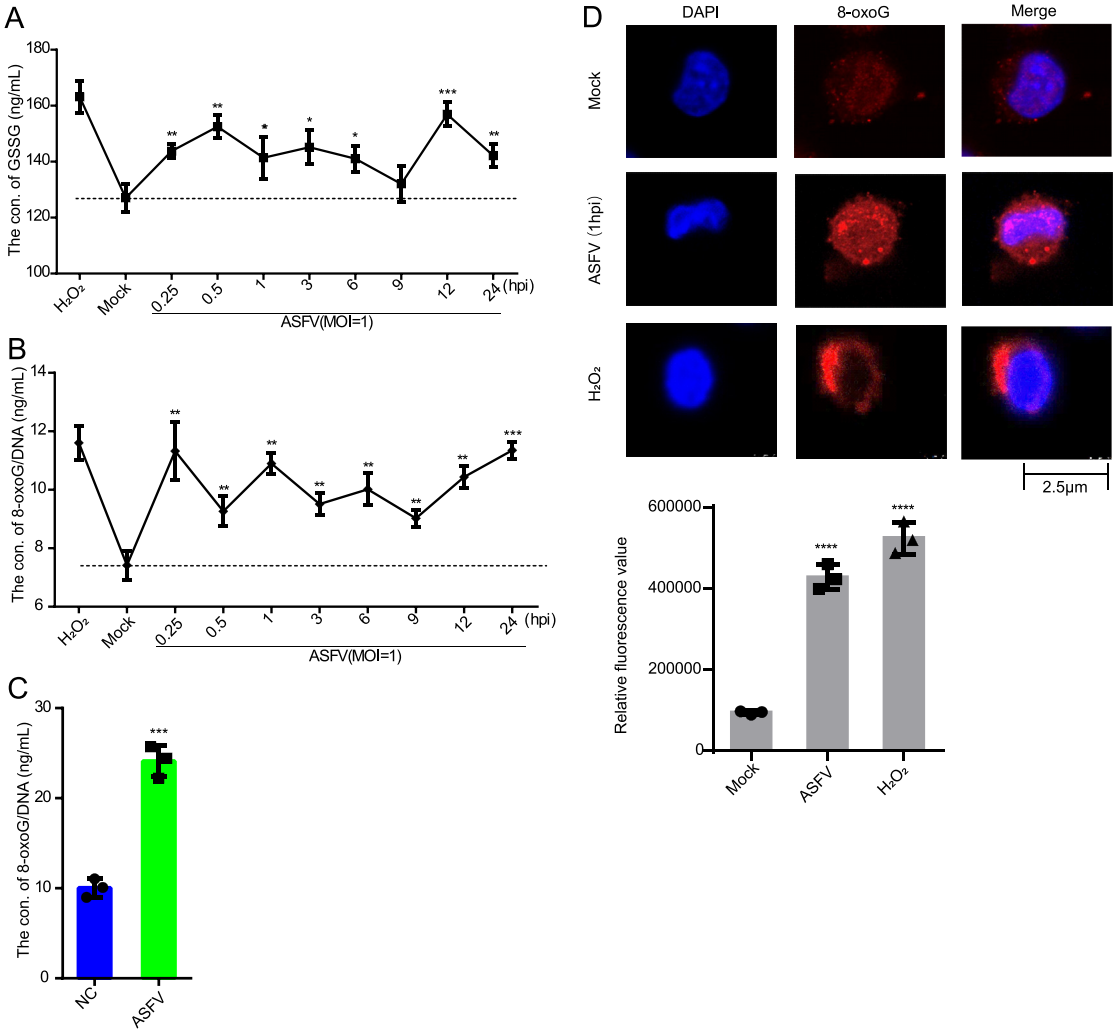

Fig. 1. ASFV infection induced dynamic changes in ROS and promoted 8-oxoG production. **A** The concentration of oxidized glutathione (GSH) disulfide (GSSG) is an indicator of the ROS level. PAMs were infected with ASFV (MOI = 1) for different times, then the samples were lysed and the cellular ROS levels were determined by using a Glutathione Oxidized (GSSG) Colorimetric Assay Kit. PAMs were stimulated with H_2O_2 (500 μmol/L) for 15 min as a positive control. **B** The production of the oxidative damage marker 8-oxoG was evaluated by ELISA at different time points post-ASFV infected PAMs (MOI = 1), and H_2O_2 (500 μmol/L) stimulation for 15 min was used as a positive control. **C** Genomic DNA was extracted from healthy (NC) and ASFV-infected lung tissue (ASFV), respectively, and the 8-oxoG levels were measured by ELISA (n = 3). **D** Representative images illustrating the production of 8-oxoG in ASFV-infected PAMs (MOI = 1) at 1 hpi. H_2O_2 (500 μmol/L) stimulation for 15 min and mock-infected PAMs were used as positive and negative control (scale bar = 2.5 μm). Data were shown as mean with standard deviation. Statistical analyses were performed by Student's *t*-test using Prism software. ****$P < 0.0001$; ***$P < 0.001$; **$P < 0.01$; *$P < 0.05$.

infected PAMs. RT-PCR results demonstrated dynamic changes of OGG1 mRNA expression in ASFV-infected PAMs from 0.5 hpi to 48 hpi, with a significant increase (5-fold) at 9 hpi (Fig. 2A). Western blot analysis revealed that OGG1 protein expression levels also varied over time, which were significantly increased at 9 hpi, slightly decreased at 12, 24 hpi, and increased again at 48 hpi (Fig. 2B). Furthermore, the production of OGG1 was measured using an OGG1 specific antibody and fluorescent secondary antibody by immunofluorescence. Fluorescence signals were detected, and fluorescence densities were higher in the ASFV-infected PAMs at 9 hpi than that in mock cells (Fig. 2C). Further research showed that the mRNA transcription level and protein expression level of OGG1 were gradually upregulated in ASFV-infected PAMs with increasing multiplicities of infection (MOIs) of 0.1, 0.5, 1, 2 or 5 at 48 hpi (Fig. 3A and C). The mRNA level of the viral *B646L* gene was also detected to demonstrate viral replication at incremental MOIs (Fig. 3B), supporting successful AFSV infection in PAMs. These data suggested that ASFV infection could induce the expression of OGG1, implying a potential role for OGG1 in ASFV infection.

3.3. ASFV infection altered the subcellular localization of OGG1 and 8-oxoG in cells

To further explore the involvement of OGG1 during ASFV infection, the expression and subcellular localization of OGG1 were evaluated upon ASFV infection in PAMs by Western blotting, and lamin B and β-tubulin were considered as nuclear and cytosolic protein controls, respectively. The results revealed that OGG1 migrated from the nucleus to the cytoplasm from 12 to 24 hpi (Fig. 4A). Furthermore, the localization of OGG1 (green) and 8-oxoG (red) in PAMs at 12 and 24 hpi was determined by immunofluorescence analysis. Similar to the immunoblot analysis results, it was found that at the early post-infection time point (12 hpi), OGG1 was scattered in both the nucleus and cytoplasm and colocalized with 8-oxoG mainly in the nucleus. At the later infection time point (24 hpi), the colocalization was mostly in the cytoplasm (Fig. 4B). Interestingly, a faint fluorescence signal was detected in mock cells, indicating that oxidative damage repair essentially occurred in PAMs. Strong signals were detected in the nucleus and cytoplasm under ASFV

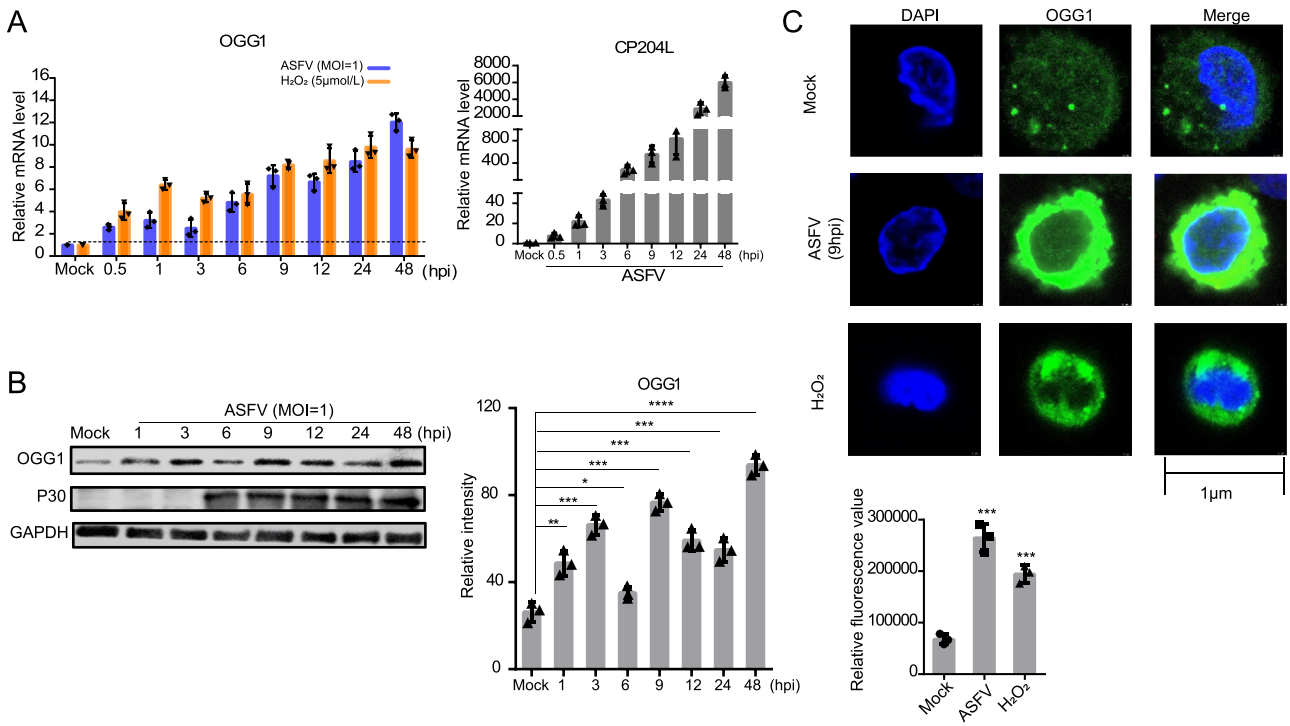

Fig. 2. The DNA repair enzyme OGG1 was elicited in PAMs by ASFV and showed dynamic expression over time. **A** RT-qPCR was used to determine the mRNA levels of *OGG1* in PAMs infected with ASFV or stimulated with H_2O_2 at different time points. The mRNA level of ASFV gene *CP204L* was used to attest the viral replication over time. *GAPDH* was served as a reference gene. **B** PAMs were mock infected or infected with ASFV (MOI = 1). At the indicated time post-infection (hpi), whole-cell extracts were prepared, and the protein levels were detected by Western blot. The relative intensity of OGG1 was standardized by GAPDH and analyzed by Image J. **C** Confocal microscopy verified the distribution of OGG1 (green) in ASFV- infected (MOI = 1) or mock infected PAMs. Nuclei were counterstained with DAPI (blue) (scale bar = 1 μm). Data were shown as mean with standard deviation. Statistical analysis was performed by Student's *t*-test. $^{****}P < 0.0001$; $^{***}P < 0.001$; $^{**}P < 0.01$; $^{*}P < 0.05$.

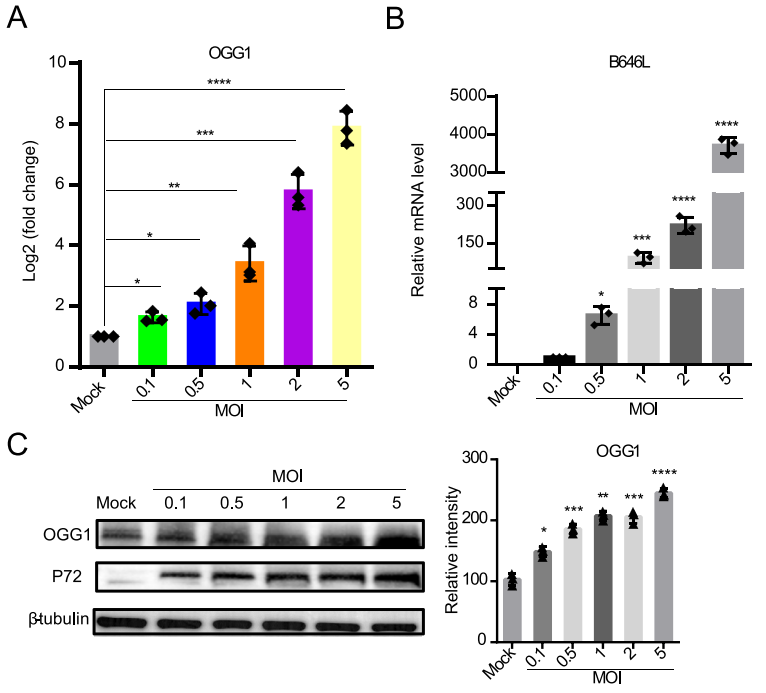

Fig. 3. The expression of OGG1 induced by ASFV was MOI-dependent. **A** RT-qPCR was used to determine the mRNA levels of *OGG1* in PAMs infected with ASFV at different MOIs of 0.1, 0.5, 1, 2 or 5 at 48 hpi. *GAPDH* was used as a reference gene. Data was quantified by using Log_2 (fold change) method and normalized with mock control. **B** The mRNA level of ASFV gene *B646L* was assessed to indicate viral replication at incremental MOIs. *GAPDH* was served as a reference gene. **C** The protein expression level of OGG1 in PAMs infected with the indicated MOI at 48 hpi was analyzed by Western blot. Data were shown as mean with standard deviation. Statistical analysis was performed by Student's *t*-test. $^{****}P < 0.0001$; $^{***}P < 0.001$; $^{**}P < 0.01$; $^{*}P < 0.05$.

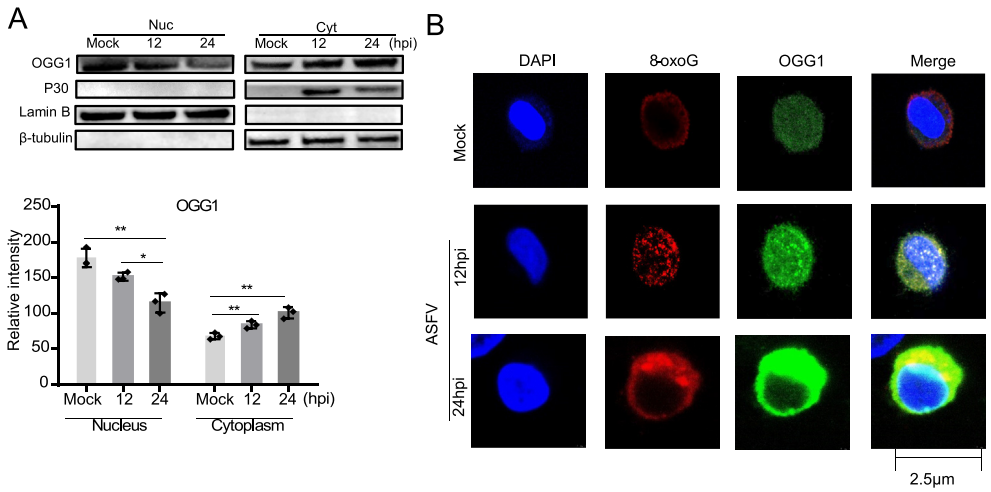

Fig. 4. ASFV altered the colocalization of OGG1 and 8-oxoG in cells. **A** PAMs were infected with ASFV (MOI = 1) for 0, 12 and 24 h, then the target proteins in the nucleus and cytoplasm were detected by Western blot. The relative intensity of OGG1 in the nucleus and cytoplasm was calibrated by Lamin B and β-tubulin, respectively. **B** PAMs were infected with ASFV (MOI = 1) and the cells were collected at 12 and 24 hpi. OGG1 and 8-oxoG were detected using specific antibodies, which were visualized with Alexa Fluor 488- or 594-conjugated secondary antibodies, respectively, using confocal microscopy. Colocalization of OGG1 (green) and 8-oxoG (red) in cells appears yellow in the merged images (scale bar = 2.5 μm). Data were shown as mean with standard deviation. Statistical analysis was performed by Student's *t*-test. $^{**}P < 0.01$; $^{*}P < 0.05$.

infection, suggesting that oxidative damage was generated in the host cell genome, including nuclear and mitochondrial DNA. This finding was of high importance, as it specifically demonstrated that BER and OGG1 were involved in ASFV infection.

3.4. Cytotoxicity of OGG1 inhibitors in PAMs

To verify the effects of OGG1 on ASFV replication, we selected two OGG1 inhibitors (TH5487 and SU0268) that have been reported in previous studies (Hanna et al., 2021; Zhang et al., 2021). The structures of the compounds are shown in Fig. 5A. First, the cytotoxicity of TH5487 and SU0268 was assessed. The CC_{50} values of TH5487 and SU0268 on PAMs were determined to be 12.94 μmol/L (95% CI = 11.16–15.11) and 37.92 μmol/L (95% CI = 28.53–41.35), respectively (Fig. 5B). In antiviral studies, to mitigate the cytotoxic effects, TH5487 and SU0268 were used at maximum concentrations of 5 and 10 μmol/L (Supplementary Fig. S2A). We further assessed whether the cytotoxicity of OGG1 inhibitors on PAMs was time dependent by treating the cells with 5 or 10 μmol/L individual OGG1 inhibitors for 0, 1, 3, 6, 9, 12 and 24 h. The results showed that the optimal concentration did not influence cell viability over an extended time (Supplementary Fig. S2B).

3.5. OGG1 inhibition suppressed ASFV proliferation

To determine whether OGG1 inhibitors can affect the replication of ASFV in PAMs, we detected the mRNA levels of the viral early gene *CP204L* and the late gene *B646L* after treatment by qRT-PCR. The data showed that TH5487 (5 μmol/L) and SU0268 (10 μmol/L) strongly suppressed the transcription of the *CP204L* gene relative to the DMSO control. Meanwhile, TH5487 exerted stronger inhibitory potency on

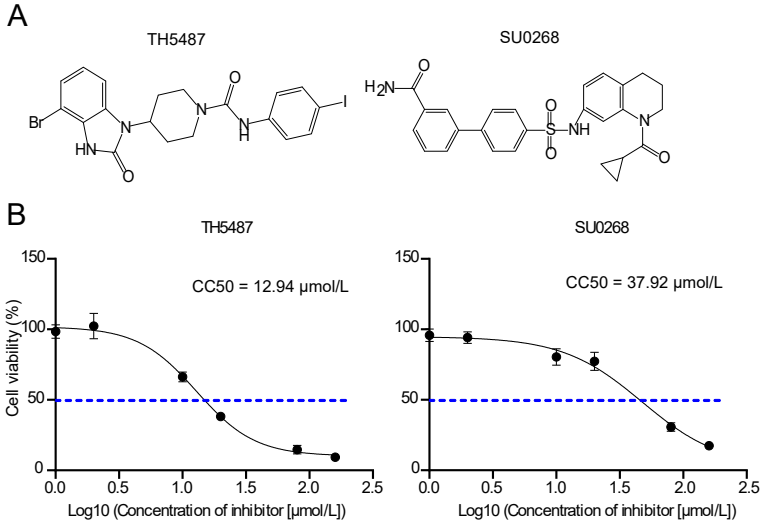

Fig. 5. Cytotoxicity of OGG1 inhibitors in PAMs. **A** Published chemical structures of TH5487 and SU0268. **B** CC_{50} values of TH5487 and SU0268 were determined by using the CCK8 Kit, and data analysis was performed using GraphPad Prism. Data were represented as the average of three independent experiments with standard deviation.

mRNA level of *B646L* compared to that of SU0268 (Fig. 6A). The duration of the effect of these two inhibitors on ASFV replication was further evaluated. PAMs were treated with SU0268 (10 μmol/L) or TH5487 (5 μmol/L) for 6 h prior to ASFV infection, and the samples were collected at 0.5, 1, 3, 6, 9, 12, and 24 hpi. The relative mRNA expression levels of *CP204L* and *B646L* were detected by qRT-PCR. As expected, the data confirmed that *CP204L* and *B646L* mRNA levels at various time points were significantly reduced in OGG1 inhibitors treated cells (Fig. 6B and C). Additionally, siRNA was used to further explore the role of silencing OGG1 on viral replication. The efficacy of siRNA targeting OGG1 transcript was firstly evaluated by qRT-PCR and Western blot (Fig. 6D and E). The significant decrease in mRNA and protein levels of ASFV genes was observed in OGG1-silencing cells (Fig. 6F and E), indicating that OGG1 knockdown downregulated ASFV replication. To further assess the function of OGG1 on the proliferation of ASFV, MA104 cells were transfected with HA-OGG1 plasmids and infected with ASFV. Western blot analysis showed that during ASFV infection, OGG1 overexpression increased ASFV replication (Fig. 6G). These suggested that OGG1 played a key role in ASFV infection and it could be a potential antiviral target.

To further determine that whether the antiviral activity of TH5487 and SU0268 against ASFV obey a dose-dependent manner, ASFV-infected PAMs were treated with two individual inhibitors at increasing concentrations. As shown in Fig. 7A and B, the viral yields were significantly decreased from 7.6 to 2.6 or 7.6 to 1 log HAD_{50}/mL at the maximum concentration of SU0268 or TH5487, respectively ($P < 0.001$). In addition, after treatment of OGG1 inhibitors, the viral titer level gradually decreased in ASFV-infected PAMs at different MOIs (0.5, 1 or 5) at 7 dpi (Fig. 7C). At the gene transcription level, *CP204L* and *B646L* mRNA transcription was significantly decreased in OGG1-suppressed cells by both OGG1 inhibitors when concentrations were >1 μmol/L ($P < 0.001$) (Fig. 7D and E). Further analysis revealed that viral p72 protein expression levels were restrained in a dose-dependent manner in ASFV-infected PAMs treated with the two inhibitors, especially upon treatment with 10 μmol/L SU0268, in which the expression of the p72 protein was almost blocked (Fig. 7F). These results demonstrated that ASFV proliferation was successfully inhibited by the OGG1 inhibitors TH5487 and SU0268 in a dose-dependent manner, implying that they are potentially reagents to restrict ASFV replication.

3.6. OGG1 inhibition downregulated the expression of ASFV-BER-associated proteins

We investigated whether the depletion of OGG1 affected ASFV-BER-associated enzyme expression in PAM cells. For this purpose, the *O174L*, *NP419L* and *E296R* mRNA and protein levels were measured in PAMs pretreated with or without OGG1 inhibitors at the indicated concentrations separately by qRT-PCR or Western blot at 24 hpi. Notably, the transcription levels of the viral genes were prominently reduced at various time points (Fig. 8A) and in a dose-dependent manner (Fig. 8B). Additionally, Western blot analysis of whole-cell extracts revealed that the protein levels ASFV-BER-associated enzymes were decreased in the presence of OGG1 inhibitors (Fig. 8C and D). Together, these results demonstrated that OGG1 was necessary for the expression of ASFV-BER associated proteins.

3.7. OGG1 coupled with ASFV MGF360-14L protein to disturb the production of IFN-β

To further understand the biological function of OGG1 in ASFV infection, a Co-IP-MS analysis was performed to screen viral proteins that potentially interacted with OGG1. After removing the non-specific binding proteins of IgG, several ASFV proteins interacted with OGG1 were identified. MGF360-14L is one of them, which has been reported to negatively regulate the production of IFN-β through the cGAS-STING pathway (Wang Y. et al., 2021). We used Co-IP assay and confocal immunofluorescence assay to verify the interaction between OGG1 and MGF360-14L. The Co-IP analysis showed that OGG1 was interacted efficiently with MGF360-14L (Fig. 9A). A confocal immunofluorescence assay showed that the OGG1 and MGF360-14L proteins colocalized in the cytoplasm (Fig. 9B). Furthermore, we found that the expression of

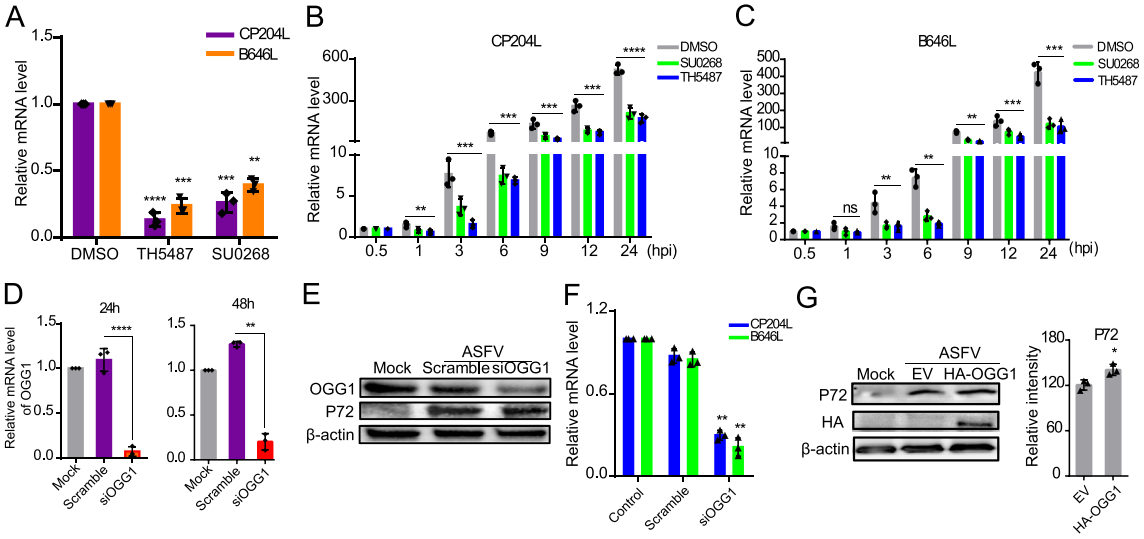

Fig. 6. OGG1 inhibition suppressed ASFV proliferation. **A** PAMs were pretreated with TH5487 (5 μmol/L) or SU0268 (10 μmol/L) for 6 h each. Then, PAMs were infected with ASFV (MOI = 1). Samples were harvested at 24 hpi. qRT-PCR was performed to analyse the mRNA level of the early viral gene *CP204L* and the late gene *B646L*. *GAPDH* was served as a reference gene. **B, C** PAMs were treated with SU0268 (10 μmol/L) or TH5487 (5 μmol/L) for 6 h prior to ASFV (MOI = 1) infection. The samples were collected at 0.5, 1, 3, 6, 9, 12, and 24 hpi. The relative expression levels of *CP204L* and *B646L* were detected by qRT-PCR. *GAPDH* was used as a reference gene. **D** OGG1 silencing in PAMs was determined by qRT-PCR, and *GAPDH* served as a reference gene. **E, F** PAMs were transfected with si-OGG1 or si-NC (scramble) for 24 h, then infected with ASFV (MOI = 1) for 24 h. The expression of viral protein was tested by Western blotting and the mRNA level of *CP204L* and *B646L* were analyzed by qRT-PCR. The control group was only infected with ASFV (MOI = 1) for 24 h. *GAPDH* was used as a reference gene. **G** MA104 cells were transfected with HA-OGG1 (2 μg) expression plasmids for 24 h and then infected with ASFV (MOI = 1) for 24 h. Western blot was performed to detect the protein level of OGG1, P72 and β-actin. Data were shown as mean with standard deviation. Statistical analysis was performed by Student's *t*-test. ****$P < 0.0001$; ***$P < 0.001$; **$P < 0.01$; *$P < 0.05$.

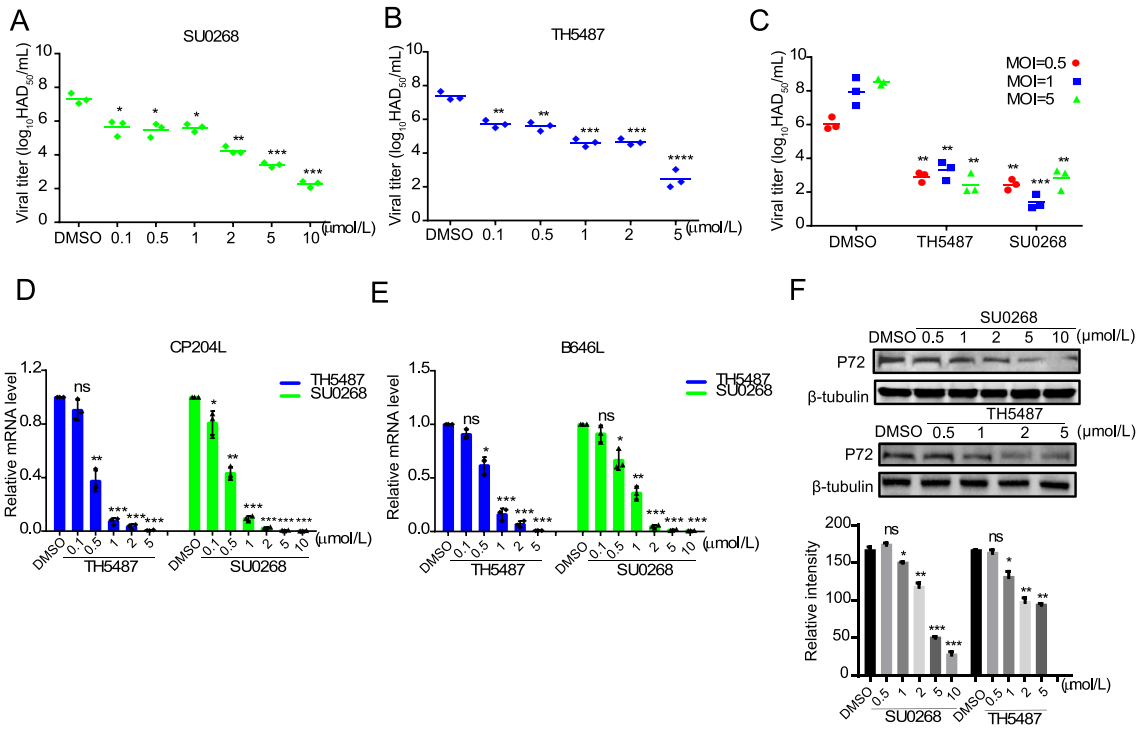

Fig. 7. ASFV yield was decreased by OGG1 inhibitors. **A, B** Titration of infectious ASFV was quantified by using the HAD assay. PAMs were pretreated with TH5487 and SU0268 for 6 h, and ASFV was then added to the cells and titrated in triplicate using 10-fold serial dilutions. HAD was determined on day 7 post-infection, and DMSO treatment was used as a negative control. **C** The viral titer was measured in PAMs after ASFV infection at MOIs of 0.5, 1 or 5 at 7 days post-infection. The viral titer was compared with that in the DMSO-treated group. **D, E** The mRNA levels of the *CP204L* and *B646L* genes were verified by qRT-PCR. PAMs were treated with TH5487 and SU0268 for 6 h prior to ASFV (MOI = 1) infection, and the samples were then collected at 24 hpi. *GAPDH* was served as a reference gene. **F** PAMs were pretreated with TH5487 and SU0268 at the indicated concentrations for 6 h, and cells were harvested after ASFV infection for 24 h. The protein level of P72 was determined by Western blot. Data were shown as mean with standard deviation. Statistical analysis was performed by Student's *t*-test. $^{****}P < 0.0001$; $^{***}P < 0.001$; $^{**}P < 0.01$; $^{*}P < 0.05$; ns, not significant.

MGF360-14L were obviously increased in both translation and transcription level with the enhancing expression of OGG1 (Fig. 9C and D). To further explore whether OGG1 was involved in production of IFN-β, si-OGG1 and two inhibitors were used. As shown in Fig. 9E and F, OGG1 inhibition significantly upregulated the mRNA levels of *IFN-β* in ASFV-infected PAMs. In summary, these data suggested that OGG1 might interact with ASFV MGF360-14L protein to further affect the production of IFN-β.

4. Discussion

The battles between the virus and host cells are crucial for the virus to start and complete productive infection. Several biological processes are viewed as potential targets in rational vaccine design or latent antiviral strategies, such as the DNA damage repair pathway. DNA damage is a common event in the cell life cycle, leading to mutation, cancer, and cell death (Kolodner et al., 2002; Puddu et al., 2019). Infection by viruses is often associated with oxidative stress and DNA damage (El-Amine et al., 2018). ROS-induced oxidative stress and complex oxidative DNA lesions are key executors in the progression of virus-induced pathogenesis, but the molecular mechanisms and biological significance of these cellular responses are poorly understood. One crucial function of ROS is to defend the cell against invading bacterial and viral pathogens (Dryden, 2018; Dryden et al., 2017). However, some viruses thrive in ROS-abundant environments, suggesting that ROS is beneficial for the virus (Paiva and Bozza, 2014). The underlying mechanism by which ROS impacts on viral replication remains to be elucidated.

ASFV is a complex double-stranded DNA virus replicating mainly in the cytoplasm of macrophages (Xian and Xiao, 2020), where release of ROS may cause the accumulation of 8-oxoG in ASFV.

Numerous studies have shown that OGG1 is involved in viral infection. OGG1 was upregulated upon EBV infection in primary B cells (Wang et al., 2020). HIV-infected patients showed increased levels of 8-oxoG and significantly decreased DNA glycosylase activity (Aukrust et al., 2005). Moreover, decreased HIV infection was associated with the decreased expression of OGG1, and the absence of OGG1 significantly reduced the efficiency of HIV integration (Bennett et al., 2014). Given the role of OGG1 in different viruses, in this study, we revealed that ASFV infection of PAMs induced ROS and DNA oxidative damage, as displayed by the contents of GSSG and 8-oxoG. We also found that ASFV infection resulted in the accumulation of genomic 8-oxoG lesions and induced dynamic changes in OGG1 expression during infection. In addition, ASFV altered the colocalization of 8-oxoG and OGG1, implying that OGG1 plays a key role in viral infection.

ASFV infection triggered heavy ROS and 8-oxoG production, which exhibited dynamic changes over time. High levels of ROS and 8-oxoG were observed early in infection, supporting the notion that the induction of oxidative stress is virus-driven. It is interesting to note that after a progressive increase peaking at 30 min post-infection, the levels of intracellular ROS gradually decreased and suddenly increased at 12 hpi. It is possible that activation of the cellular antioxidant machinery may contribute to a balance of redox reactions, together with the expression of viral proteins that inhibit oxidative stress. The formation of viral factories and the accumulation of a large number of intermediate and late viral proteins (Gaudreault et al., 2020) possibly stimulated ROS production again after 9 hpi (Fig. 1).

Viral replication entailed a higher oxidant environment, leading to oxidative damage not only to host cells but also to viral genomes (Novoa et al., 2005). To protect against oxidative damage, similar to some other nucleocytoplasmic large DNA viruses, ASFV evolved a BER process to

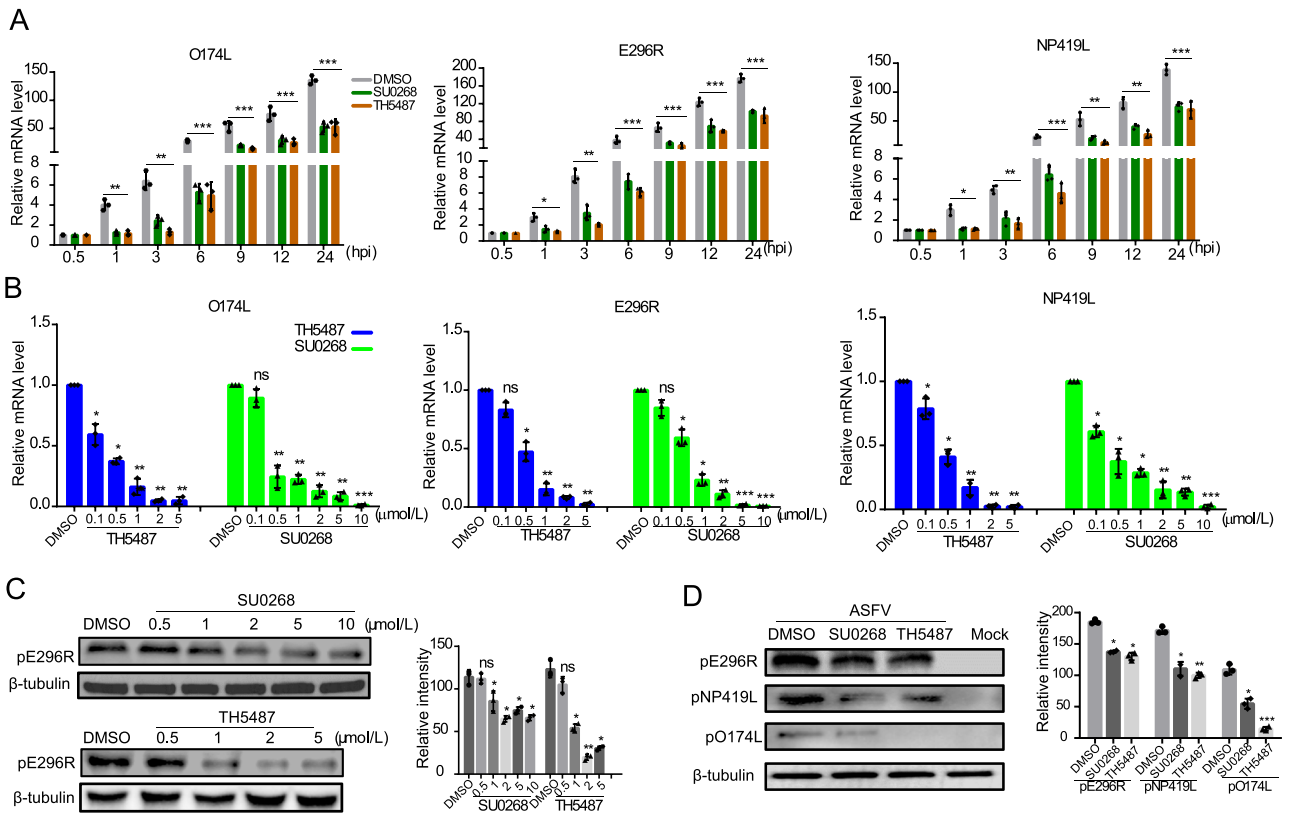

Fig. 8. The expression of ASFV-BER-associated proteins was inhibited by OGG1 inhibitors. **A** PAMs were pretreated with TH5487 (5 μmol/L) or SU0268 (10 μmol/L) for 6 h. ASFV-BER-associated protein (pO174L, pNP419L and pE296R) mRNA levels were determined by RT-PCR at different time points after ASFV (MOI = 1) infection. The expressed significance was compared with 0.5 hpi. *GAPDH* was served as a reference gene. **B** PAMs were pretreated with TH5487 or SU0268 at assigned concentrations for 6 h and then harvested after ASFV (MOI = 1) infection at 24 hpi. The mRNA levels were assessed by qRT-PCR. *GAPDH* was used as a reference gene. **C, D** PAMs were pretreated with OGG1 inhibitors at the indicated concentrations for 6 h. At 24 hpi, mock- and ASFV-infected (MOI = 1) cells were lysed, and ASFV-BER protein levels were assessed by Western blot analysis using specific antibodies. The relative intensity was calibrated by β-tubulin. Data were shown as mean with standard deviation. Statistical analysis was performed by Student's *t*-test. $^{****}P < 0.0001$; $^{***}P < 0.001$; $^{**}P < 0.01$; $^{*}P < 0.05$; ns, not significant.

maintain the integrity of the viral genome in the highly oxidative and potentially mutagenic environment of swine macrophages (Dixon et al., 2013; Iyer et al., 2001). Since there is currently no annotated DNA glycosylase gene for specifically recognizing 8-oxoG from ASFV DNA, it is possible that the virus uses a cellular enzyme to initiate its BER, implying OGG1 may has pivotal role in ASFV infection. Thus, we determined the change in OGG1 and observed its cellular localization with 8-oxoG, and we found that it was involved in ASFV infection. The level of OGG1 in PAM cells post-ASFV infection was confirmed by qRT-PCR and Western blot assays to be significantly higher than that in uninfected cells and presented a dynamic change over time that was compatible with the rapid increase in 8-oxoG in virus-infected cells. This may be because OGG1 was elicited to respond to oxidative damage and activate the BER pathway in host cells (Fig. 2). The combination of OGG1 and 8-oxoG was observed, and the displacement of OGG1 and 8-oxoG colocalization from the nucleus to the cytoplasm suggested that OGG1 likely performed different functions in different periods of viral infection (Fig. 4). ASFV-induced DNA oxidative damage may exist in both the nucleus and mitochondria, even in virus genomes. The presence of such damage can in turn directly or indirectly modulate cellular signal transduction pathways (Sampath and Lloyd, 2019), thereby affecting the replication of the virus. Previous studies have shown that OGG1 is imported to mitochondria to prevent oxidant-induced mitochondrial dysfunction, p53 mitochondrial translocation, and intrinsic apoptosis (Kim et al., 2014). Induction of the apoptosis pathway is a common cellular DDR to viral infection, which has the effect of limiting the replication and spread of viral progeny. This may suggest a multilayered mechanism aimed at manipulating the OGG1-dependent DDR after ASFV infection by constraining the enzyme activity and altering its localization. Taken together, OGG1 appears to be a key cellular factor involved in ASFV replication by regulating DNA damage responses.

Indeed, recent studies have demonstrated that the BER pathway plays an essential role in large DNA viruses, and suppression of DNA repair may be a crucial target through which to counteract viruses (Weitzman and Fradet-Turcotte, 2018). Especially, DNA glycosylase, which recognizes and excises the damaged bases, has been evaluated as a therapeutic target in virus-induced cancer therapy (Redrejo-Rodriguez and Salas, 2014). Due to the essential role of OGG1 in the BER pathway, we selected inhibitors of OGG1 to verify the effects of OGG1 on ASFV replication. Interestingly, we found that TH5487 and SU0268 significantly impaired ASFV proliferation (Figs. 6–8). Moreover, we found that OGG1 could interact with MGF360-14L, which is a member of the MGF360 family. Previous studies have shown that ASFV MGFs families suppress the host immune response through disturbing IFNs signal pathway, and MGF360-14L was involved in suppressing type I IFN induction (Rathakrishnan et al., 2022; Reis et al., 2016). Our data showed that inhibition of OGG1 upregulated the transcription of IFN-β, indicating that ASFV may disturb IFN-β production by interacting with OGG1, thus creating a favorable condition for self-proliferation and diffusion.

According to a report, OGG1 is a multifunctional DNA glycosylase; upon oxidative stress or during inflammation, the increased levels of ROS transiently inhibit OGG1 enzymatic activity (Pan et al., 2017), and OGG1 becomes a chromatin recruiter of transcription factors, regulating gene

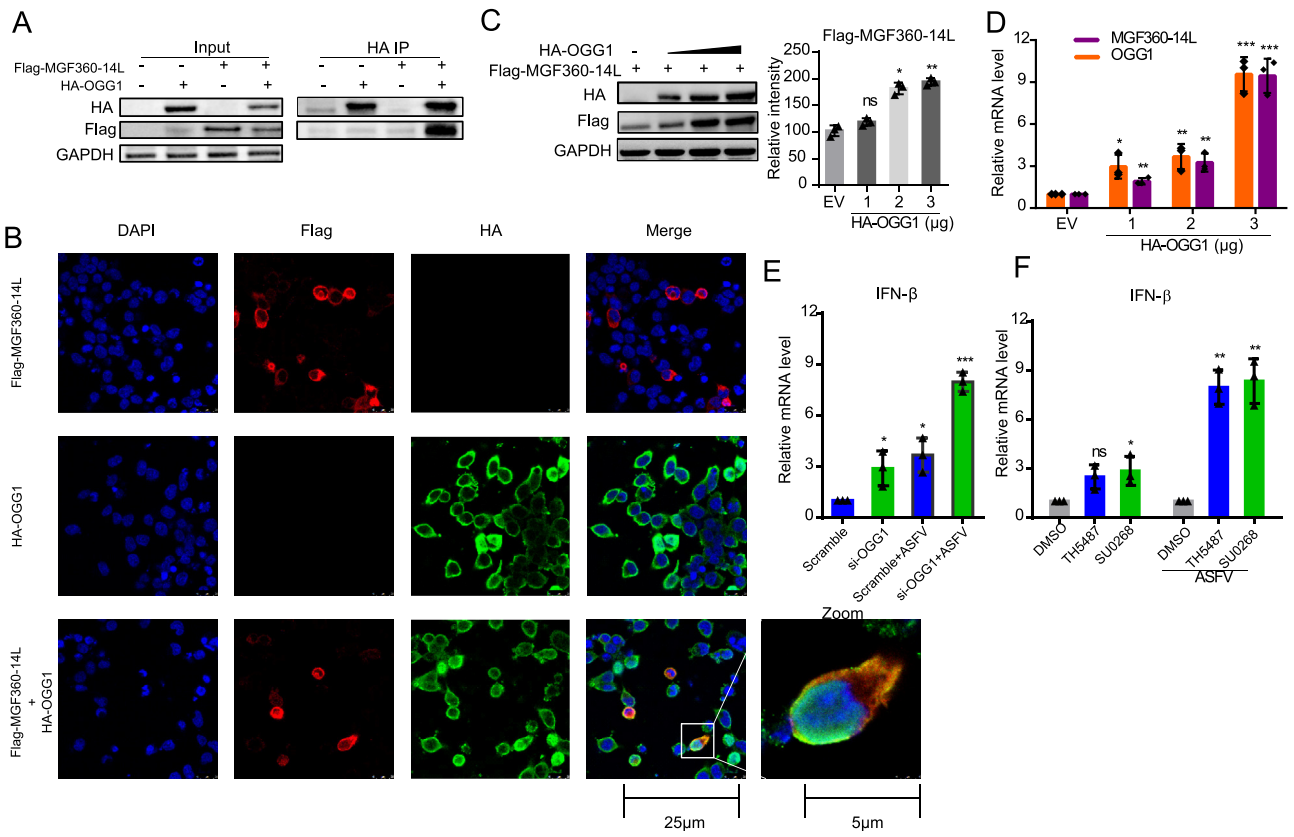

Fig. 9. OGG1 interacted with ASFV MGF360-14L and affected IFN-β transcription. **A** HA-OGG1 (2 μg) and Flag-MGF360-14L (2 μg) plasmids were cotransfected into MA104 cells for 24 h. The interaction was analyzed through Co-IP using anti-Flag and anti-HA antibodies. **B** MA104 cells were transfected with HA-OGG1 and Flag-MGF360–14L expression plasmids for 24 h. Double immunofluorescent staining revealed colocalization of HA-OGG1 (green) and Flag-MGF360-14 L (red) in cells (scale bar = 25 μm). **C** MA104 cells were cotransfected with Flag-MGF360-14L (1 μg) and HA-OGG1 (0, 1, 2, 3 μg) for 24 h. Then cells were lysed and tested by Western blotting. **D** MA104 cells were transfected with HA-OGG1 (0, 1, 2, 3 μg) for 12 h, then infected with ASFV (MOI = 1) for 24 h. The mRNA level of ASFV *MGF360-14L* was analyzed by qRT-PCR. *GAPDH* was used as a reference gene. **E** PAMs were transfected with si-OGG1 or si-NC (scramble) for 24 h and then infected with or without ASFV (MOI = 1) for 24 h. *IFN-β* mRNA level was detected by qRT-PCR. *GAPDH* was served as a reference gene. **F** PAMs were pretreated with 5 μmol/L TH5487, or 10 μmol/L SU0268 for 6 h and then infected with ASFV (MOI = 1) for 24 h. The transcription level of *IFN-β* was determined by qRT-PCR. *GAPDH* was used as a reference gene. Data were shown as mean with standard deviation. Statistical analysis was performed by Student's *t*-test. ***$P < 0.001$; **$P < 0.01$; *$P < 0.05$; ns, not significant.

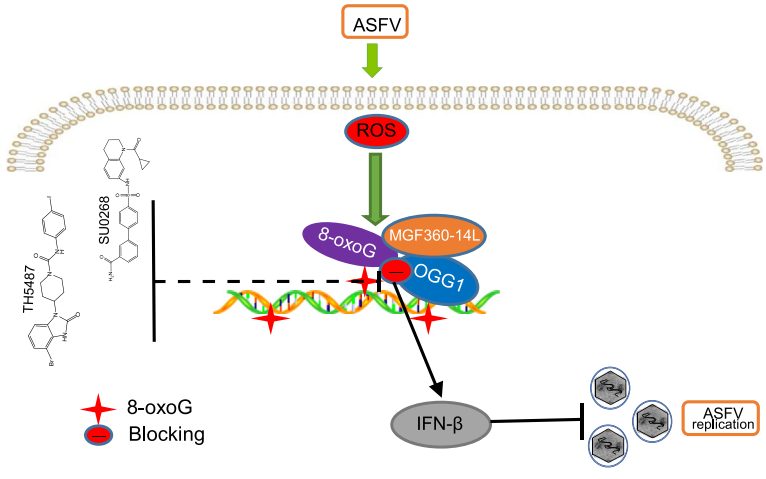

Fig. 10. A mechanism of OGG1 inhibitors suppresses ASFV replication. ASFV infection triggers dynamic changes in ROS and 8-oxoG and consistently increases the expression of DNA repair enzyme OGG1. The small-molecule inhibitors TH5487 and SU0268 block OGG1 binding to 8-oxoG which then upregulated IFN-β transcription and thus to suppress ASFV replication. Additionally, the interaction of OGG1 with viral MGF360-14L protein could disturb IFN-β production to further affect ASFV replication.

transcription (Ba et al., 2014; D'Augustin et al., 2020). TH5487 and SU0268 may directly block OGG1 from exerting the biological functions by inhibiting protein-DNA substrate binding (Qin et al., 2020; Baquero et al., 2021). The novel small-molecule TH5487 was designed as a potent and selective active site inhibitor of OGG1 that prevents OGG1 from binding to its DNA substrate and alters OGG1-chromatin dynamics and OGG1 recruitment kinetics. TH5487 not only prevents the binding of OGG1 to damaged DNA but also inhibits its catalytic function, impairing OGG1 incision and the generation of DNA breaks (Hanna et al., 2020). Moreover, the tetrahydroquinoline compound SU0268 was confirmed to be selective for inhibiting OGG1 over other BER enzymes, which inhibits DNA binding and base excision. SU0268 could engage OGG1 and inhibit its activity, resulting in an increase in the accumulation of 8-oxoG (Kant et al., 2021). Therefore, there are at least three possibilities that could account for how these compounds inhibit ASFV by blocking OGG1 function. First, they can only inhibit catalytic activity, reducing glycosidic bond cleavage, such that AP sites might not generated and strand scission by OGG1 cannot occur during BER, further influencing OGG1-BER enzymatic activity-dependent promoter activation (Pan et al., 2016). Second, they could inhibit OGG1, another epigenetic regulator, by preventing OGG1 from binding to DNA substrates and recruiting chromatin remodelers, further altering chromatin modifications and, thus, regulating gene expression in the host (Xia et al., 2017). Third, they may block OGG1 from being hijacked and interacting with viral proteins, ASFV MGF360-14L in this study, disturbing the type I IFN pathway. Thus, our data suggest that the primary mode of TH5487 or SU0268 impaired ASFV replication by upregulating IFN-β production.

5. Conclusions

In conclusion, our study investigated the changes in biomarkers of oxidative stress and oxidative damage repair processes during ASFV infection. Meanwhile, we demonstrated that OGG1 inhibition with TH5487 and SU0268 could upregulated IFN-β transcription and thus to suppress ASFV replication. Additionally, the interaction of OGG1 with viral MGF360-14L protein might disturb IFN-β production to further affect ASFV replication (Fig. 10). Taken together, our results provide novel insight into ASFV pathogenesis with emphasis on the oxidative and antiviral roles of the OGG1 inhibitors SU0268 and TH5487 in PAM cells after the onset of ASFV infection. Further clinical trials will be needed to determine whether the compounds will benefit farm pigs as a preventive antiviral agent. The discovery and development of highly potent, selective, and stable small-molecule inhibitors of OGG1 against ASFV infection, as well as determination of the relative regulatory mechanism of OGG1, remain important goals for further study.

Data availability

All data generated or analyzed during the current study are included in this article and its supplementary information files.

Ethics statement

All experiments with live ASFV operations were performed in a biosafety level-3 (BSL-3) laboratory in the Lanzhou Veterinary Research Institute (LVRI), Chinese Academy of Agriculture and Sciences (CAAS), accredited by the China National Accreditation Service for Conformity Assessment (CNAS) and approved by the Ministry of Agriculture and Rural Affairs. In the laboratory, to reduce any potential risk, the protocols are strictly followed, and all activities are monitored by the professional staff at LVRI and randomly inspected by local and central governmental authorities without advance notice. This study was approved by the Animal Ethics Committee of the Lanzhou Veterinary Research Institute, Chinese Academy of Agricultural Sciences. All animals were handled in accordance with the Animal Ethics Procedures and Guidelines of the People's Republic of China.

Author contributions

Jie Fan: data curation, methodology and writing-original draft preparation. Xinqian Lv: validation, investigation. Saixia Yang: visualization, methodology. Shuxian Geng: formal analysis. Jifei Yang: software. Yaru Zhao: validation. Zhonghui Zhang: software. Zhijie Liu: project administration. Guiquan Guan: reviewing. Jianxun Luo: supervision. Qiaoying Zeng: software, validation. Hong Yin: funding acquisition, supervision. Qingli Niu: conceptualization, project administration, writing-reviewing and editing.

Conflict of interest

The authors declare that they have no competing interests.

Acknowledgements

We thank Dr. Wenjing Hao (Institute of Genetics and Developmental Biology, Chinese Academy of Sciences, Beijing, China) for editing the manuscript and for her critical suggestions. This study was financially supported by the National Key Research and Development Program (Grant No. 2021YFD1800101); the National Natural Science Foundation of China (Grant No.32072830); Gansu Provincial Major project for science and technology development (Grant No. 20ZD7NA006); State Key Laboratory of Veterinary Etiological Biology, Lanzhou Veterinary Research Institute, Chinese Academy of Agricultural Sciences (Grant No. SKLVEB2020CGPY02); Natural Science Foundation of Gansu Province (Grant No. 21JR1RA214; 21JR7RA018); Basic scientific research business expenses budget incremental project, Chinese Academy of Agricultural Sciences, Lanzhou Veterinary Research Institute (Grant Nos 1610312021002) and National Agricultural Science and Technology Innovation Program (CAAS-ASTIP-2016-LVRI).

Appendix A. Supplementary data

Supplementary data to this article can be found online at https://doi.org/10.1016/j.virs.2022.11.006.

References

Alejo, A., Matamoros, T., Guerra, M., Andres, G., 2018. A proteomic Atlas of the African swine fever virus particle. J. Virol. 92, e00119–e00120.

Anand, S.K., Sharma, A., Singh, N., Kakkar, P., 2020. Entrenching role of cell cycle checkpoints and autophagy for maintenance of genomic integrity. DNA Repair 86, 102748.

Aukrust, P., Luna, L., Ueland, T., Johansen, R.F., Muller, F., Froland, S.S., Seeberg, E.C., Bjoras, M., 2005. Impaired base excision repair and accumulation of oxidative base lesions in CD4+ T cells of HIV-infected patients. Blood 105, 4730–4735.

Ba, X., Bacsi, A., Luo, J., Aguilera-Aguirre, L., Zeng, X., Radak, Z., Brasier, A.R., Boldogh, I., 2014. 8-oxoguanine DNA glycosylase-1 augments proinflammatory gene expression by facilitating the recruitment of site-specific transcription factors. J. Immunol. 192, 2384–2394.

Baquero, J.M., Benitez-Buelga, C., Rajagopal, V., Zhenjun, Z., Torres-Ruiz, R., Muller, S., Hanna, B., Loseva, O., Wallner, O., Michel, M., Rodriguez-Perales, S., Gad, H., Visnes, T., Helleday, T., Benitez, J., Osorio, A., 2021. Small molecule inhibitor of OGG1 blocks oxidative DNA damage repair at telomeres and potentiates methotrexate anticancer effects. Sci. Rep. 11, 3490.

Bennett, G.R., Peters, R., Wang, X.H., Hanne, J., Sobol, R.W., Bundschuh, R., Fishel, R., Yoder, K.E., 2014. Repair of oxidative DNA base damage in the host genome influences the HIV integration site sequence preference. PLoS One 9, e103164.

Cackett, G., Matelska, D., Sykora, M., Portugal, R., Malecki, M., Bahler, J., Dixon, L., Werner, F., 2020. The African swine fever virus transcriptome. J. Virol. 94, e00119–e00120.

Cardoso, T.C., Rosa, A.C., Ferreira, H.L., Okamura, L.H., Oliveira, B.R., Vieira, F.V., Silva-Frade, C., Gameiro, R., Flores, E.F., 2016. Bovine herpesviruses induce different cell death forms in neuronal and glial-derived tumor cell cultures. J. Neurovirol. 22, 725–735.

Chen, Y., Chen, X., Huang, Q., Shao, Z., Gao, Y., Li, Y., Yang, C., Liu, H., Li, J., Wang, Q., Ma, J., Zhang, Y.Z., Gu, Y., Gan, J., 2020. A unique DNA-binding mode of African swine fever virus AP endonuclease. Cell Discov 6, 13.

Cuesta-Geijo, M.A., Garcia-Dorival, I., Del, P.A., Urquiza, J., Galindo, I., Barrado-Gil, L., Lasala, F., Cayuela, A., Sorzano, C., Gil, C., Delgado, R., Alonso, C., 2022. New insights into the role of endosomal proteins for African swine fever virus infection. PLoS Pathog. 18, e1009784.

D'Augustin, O., Huet, S., Campalans, A., Radicella, J.P., 2020. Lost in the crowd: how does human 8-oxoguanine DNA glycosylase 1 (OGG1) find 8-oxoguanine in the genome? Int. J. Mol. Sci. 21, 8360.
Dixon, L.K., Chapman, D.A., Netherton, C.L., Upton, C., 2013. African swine fever virus replication and genomics. Virus Res. 173, 3–14.
Dryden, M., 2018. Reactive oxygen species: a novel antimicrobial. Int. J. Antimicrob. Agents 51, 299–303.
Dryden, M.S., Cooke, J., Salib, R.J., Holding, R.E., Biggs, T., Salamat, A.A., Allan, R.N., Newby, R.S., Halstead, F., Oppenheim, B., Hall, T., Cox, S.C., Grover, L.M., Al-Hindi, Z., Novak-Frazer, L., Richardson, M.D., 2017. Reactive oxygen: a novel antimicrobial mechanism for targeting biofilm-associated infection. J Glob Antimicrob Resist 8, 186–191.
El-Amine, R., Germini, D., Zakharova, V.V., Tsfasman, T., Sheval, E.V., Louzada, R., Dupuy, C., Bilhou-Nabera, C., Hamade, A., Najjar, F., Oksenhendler, E., Lipinski, M., Chernyak, B.V., Vassetzky, Y.S., 2018. HIV-1 Tat protein induces DNA damage in human peripheral blood B-lymphocytes via mitochondrial ROS production. Redox Biol. 15, 97–108.
Gaudreault, N.N., Madden, D.W., Wilson, W.C., Trujillo, J.D., Richt, J.A., 2020. African swine fever virus: an emerging DNA Arbovirus. Front. Vet. Sci. 7, 215.
Hanna, B., Helleday, T., Mortusewicz, O., 2020. OGG1 inhibitor TH5487 alters OGG1 chromatin dynamics and prevents incisions. Biomolecules 10, 1483.
Hanna, B., Michel, M., Helleday, T., Mortusewicz, O., 2021. NEIL1 and NEIL2 are recruited as potential backup for OGG1 upon OGG1 depletion or inhibition by TH5487. Int. J. Mol. Sci. 22, 4542.
Hu, S., Sheng, W.S., Schachtele, S.J., Lokensgard, J.R., 2011. Reactive oxygen species drive herpes simplex virus (HSV)-1-induced proinflammatory cytokine production by murine microglia. J. Neuroinflammation 8, 123.
Iyer, L.M., Aravind, L., Koonin, E.V., 2001. Common origin of four diverse families of large eukaryotic DNA viruses. J. Virol. 75, 11720–11734.
Jezewska, M.J., Marcinowicz, A., Lucius, A.L., Bujalowski, W., 2006. DNA polymerase X from African swine fever virus: quantitative analysis of the enzyme-ssDNA interactions and the functional structure of the complex. J. Mol. Biol. 356, 121–141.
Kant, M., Tahara, Y.K., Jaruga, P., Coskun, E., Lloyd, R.S., Kool, E.T., Dizdaroglu, M., 2021. Inhibition by tetrahydroquinoline sulfonamide derivatives of the activity of human 8-oxoguanine DNA glycosylase (OGG1) for several products of oxidatively induced DNA base lesions. ACS Chem. Biol. 16, 45–51.
Kim, S.J., Cheresh, P., Williams, D., Cheng, Y., Ridge, K., Schumacker, P.T., Weitzman, S., Bohr, V.A., Kamp, D.W., 2014. Mitochondria-targeted Ogg1 and aconitase-2 prevent oxidant-induced mitochondrial DNA damage in alveolar epithelial cells. J. Biol. Chem. 289, 6165–6176.
Kolodner, R.D., Putnam, C.D., Myung, K., 2002. Maintenance of genome stability in Saccharomyces cerevisiae. Science 297, 552–557.
Lamarche, B.J., Showalter, A.K., Tsai, M.D., 2005. An error-prone viral DNA ligase. Biochemistry 44, 8408–8417.
Malmquist, W.A., Hay, D., 1960. Hemadsorption and cytopathic effect produced by African Swine Fever virus in swine bone marrow and buffy coat cultures. Am. J. Vet. Res. 21, 104–108.
Nakabeppu, Y., Tsuchimoto, D., Ichinoe, A., Ohno, M., Ide, Y., Hirano, S., Yoshimura, D., Tominaga, Y., Furuichi, M., Sakumi, K., 2004. Biological significance of the defense mechanisms against oxidative damage in nucleic acids caused by reactive oxygen species: from mitochondria to nuclei. Ann. N. Y. Acad. Sci. 1011, 101–111.
Novoa, R.R., Calderita, G., Arranz, R., Fontana, J., Granzow, H., Risco, C., 2005. Virus factories: associations of cell organelles for viral replication and morphogenesis. Biol. Cell. 97, 147–172.
Owen, J.B., Butterfield, D.A., 2010. Measurement of oxidized/reduced glutathione ratio. Methods Mol. Biol. 648, 269–277.
Paiva, C.N., Bozza, M.T., 2014. Are reactive oxygen species always detrimental to pathogens? Antioxidants Redox Signal. 20, 1000–1037.
Pan, L., Hao, W., Zheng, X., Zeng, X., Ahmed, A.A., Boldogh, I., Ba, X., 2017. OGG1-DNA interactions facilitate NF-kappaB binding to DNA targets. Sci. Rep. 7, 43297.
Pan, L., Zhu, B., Hao, W., Zeng, X., Vlahopoulos, S.A., Hazra, T.K., Hegde, M.L., Radak, Z., Bacsi, A., Brasier, A.R., Ba, X., Boldogh, I., 2016. Oxidized guanine base lesions function in 8-oxoguanine DNA glycosylase-1-mediated epigenetic regulation of nuclear factor kappaB-driven gene expression. J. Biol. Chem. 291, 25553–25566.
Pao, P.C., Patnaik, D., Watson, L.A., Gao, F., Pan, L., Wang, J., Adaikkan, C., Penney, J., Cam, H.P., Huang, W.C., Pantano, L., Lee, A., Nott, A., Phan, T.X., Gjoneska, E., Elmsaouri, S., Haggarty, S.J., Tsai, L.H., 2020. HDAC1 modulates OGG1-initiated oxidative DNA damage repair in the aging brain and Alzheimer's disease. Nat. Commun. 11, 2484.
Piciocchi, M., Cardin, R., Cillo, U., Vitale, A., Cappon, A., Mescoli, C., Guido, M., Rugge, M., Burra, P., Floreani, A., Farinati, F., 2016. Differential timing of oxidative DNA damage and telomere shortening in hepatitis C and B virus-related liver carcinogenesis. Transl. Res. 168, 122–133.
Puddu, F., Herzog, M., Selivanova, A., Wang, S., Zhu, J., Klein-Lavi, S., Gordon, M., Meirman, R., Millan-Zambrano, G., Ayestaran, I., Salguero, I., Sharan, R., Li, R., Kupiec, M., Jackson, S.P., 2019. Genome architecture and stability in the Saccharomyces cerevisiae knockout collection. Nature 573, 416–420.
Qin, S., Lin, P., Wu, Q., Pu, Q., Zhou, C., Wang, B., Gao, P., Wang, Z., Gao, A., Overby, M., Yang, J., Jiang, J., Wilson, D.L., Tahara, Y.K., Kool, E.T., Xia, Z., Wu, M., 2020. Small-molecule inhibitor of 8-oxoguanine DNA glycosylase 1 regulates inflammatory responses during Pseudomonas aeruginosa infection. J. Immunol. 205, 2231–2242.
Rathakrishnan, A., Connell, S., Petrovan, V., Moffat, K., Goatley, L.C., Jabbar, T., Sanchez-Cordon, P.J., Reis, A.L., Dixon, L.K., 2022. Differential effect of deleting members of African swine fever virus multigene families 360 and 505 from the genotype II Georgia 2007/1 isolate on virus replication, virulence, and induction of protection. J. Virol. 96, e0189921.
Reis, A.L., Abrams, C.C., Goatley, L.C., Netherton, C., Chapman, D.G., Sanchez-Cordon, P., Dixon, L.K., 2016. Deletion of African swine fever virus interferon inhibitors from the genome of a virulent isolate reduces virulence in domestic pigs and induces a protective response. Vaccine 34, 4698–4705.
Redrejo-Rodriguez, M., Salas, M.L., 2014. Repair of base damage and genome maintenance in the nucleo-cytoplasmic large DNA viruses. Virus Res. 179, 12–25.
Ruiz-Gonzalvo, F., Rodriguez, F., Escribano, J.M., 1996. Functional and immunological properties of the baculovirus-expressed hemagglutinin of African swine fever virus. Virology 218, 285–289.
Sun, H., Niu, Q., Yang, J., Zhao, Y., Tian, Z., Fan, J., Zhang, Z., Wang, Y., Geng, S., Zhang, Y., Guan, G., Williams, D., Luo, J., Yin, H., Liu, Z., 2021. Transcriptome profiling reveals features of immune response and metabolism of Acutely infected, dead and Asymptomatic infection of African swine fever virus in pigs. Front. Immunol. 12, 808545.
Sampath, H., Lloyd, R.S., 2019. Roles of OGG1 in transcriptional regulation and maintenance of metabolic homeostasis. DNA Repair 81, 102667.
Schachtele, S.J., Hu, S., Little, M.R., Lokensgard, J.R., 2010. Herpes simplex virus induces neural oxidative damage via microglial cell Toll-like receptor-2. J. Neuroinflammation 7, 35.
Shibutani, S., Takeshita, M., Grollman, A.P., 1991. Insertion of specific bases during DNA synthesis past the oxidation-damaged base 8-oxodG. Nature 349, 431–434.
Simoes, M., Martins, C., Ferreira, F., 2013. Host DNA damage response facilitates African swine fever virus infection. Vet. Microbiol. 165, 140–147.
Tahara, Y.K., Auld, D., Ji, D., Beharry, A.A., Kietrys, A.M., Wilson, D.L., Jimenez, M., King, D., Nguyen, Z., Kool, E.T., 2018. Potent and selective inhibitors of 8-oxoguanine DNA glycosylase. J. Am. Chem. Soc. 140, 2105–2114.
Verhalen, B., Justice, J.L., Imperiale, M.J., Jiang, M., 2015. Viral DNA replication-dependent DNA damage response activation during BK polyomavirus infection. J. Virol. 89, 5032–5039.
Visnes, T., Benitez-Buelga, C., Cazares-Korner, A., Sanjiv, K., Hanna, B., Mortusewicz, O., Rajagopal, V., Albers, J.J., Hagey, D.W., Bekkhus, T., Eshtad, S., Baquero, J.M., Masuyer, G., Wallner, O., Muller, S., Pham, T., Gokturk, C., Rasti, A., Suman, S., Torres-Ruiz, R., Sarno, A., Wiita, E., Homan, E.J., Karsten, S., Marimuthu, K., Michel, M., Koolmeister, T., Scobie, M., Loseva, O., Almlof, I., Unterlass, J.E., Pettke, A., Bostrom, J., Pandey, M., Gad, H., Herr, P., Jemth, A.S., El, A.S., Kalderen, C., Rodriguez-Perales, S., Benitez, J., Krokan, H.E., Altun, M., Stenmark, P., Berglund, U.W., Helleday, T., 2020. Targeting OGG1 arrests cancer cell proliferation by inducing replication stress. Nucleic Acids Res. 48, 12234–12251.
Visnes, T., Cazares-Korner, A., Hao, W., Wallner, O., Masuyer, G., Loseva, O., Mortusewicz, O., Wiita, E., Sarno, A., Manoilov, A., Astorga-Wells, J., Jemth, A.S., Pan, L., Sanjiv, K., Karsten, S., Gokturk, C., Grube, M., Homan, E.J., Hanna, B., Paulin, C., Pham, T., Rasti, A., Berglund, U.W., von Nicolai, C., Benitez-Buelga, C., Koolmeister, T., Ivanic, D., Iliev, P., Scobie, M., Krokan, H.E., Baranczewski, P., Artursson, P., Altun, M., Jensen, A.J., Kalderen, C., Ba, X., Zubarev, R.A., Stenmark, P., Boldogh, I., Helleday, T., 2018. Small-molecule inhibitor of OGG1 suppresses proinflammatory gene expression and inflammation. Science 362, 834–839.
Wang, J., Nagy, N., Masucci, M.G., 2020. The Epstein-Barr virus nuclear antigen-1 upregulates the cellular antioxidant defense to enable B-cell growth transformation and immortalization. Oncogene 39, 603–616.
Wang, K., Maayah, M., Sweasy, J.B., Alnajjar, K.S., 2021. The role of cysteines in the structure and function of OGG1. J. Biol. Chem. 296, 100093.
Wang, R., Hao, W., Pan, L., Boldogh, I., Ba, X., 2018. The roles of base excision repair enzyme OGG1 in gene expression. Cell. Mol. Life Sci. 75, 3741–3750.
Wang, W., Ma, Y., Huang, M., Liang, W., Zhao, X., Li, Q., Wang, S., Hu, Z., He, L., Gao, T., Chen, J., Pan, F., Guo, Z., 2021. Asymmetrical arginine dimethylation of histone H4 by 8-oxog/OGG1/PRMT1 is essential for oxidative stress-induced transcription activation. Free Radic. Biol. Med. 164, 175–186.
Wang, Y., Cui, S., Xin, T., Wang, X., Yu, H., Chen, S., Jiang, Y., Gao, X., Jiang, Y., Guo, X., Jia, H., Zhu, H., 2021. African swine fever virus MGF360-14L negatively regulates type I interferon signaling by targeting IRF3. Front. Cell. Infect. Microbiol. 11, 818969.
Weitzman, M.D., Fradet-Turcotte, A., 2018. Virus DNA replication and the host DNA damage response. Annu Rev Virol 5, 141–164.
Weitzman, M.D., Lilley, C.E., Chaurushiya, M.S., 2010. Genomes in conflict: maintaining genome integrity during virus infection. Annu. Rev. Microbiol. 64, 61–81.
Xia, L., Huang, W., Bellani, M., Seidman, M.M., Wu, K., Fan, D., Nie, Y., Cai, Y., Zhang, Y.W., Yu, L.R., Li, H., Zahnow, C.A., Xie, W., Chiu, Y.R., Rassool, F.V., Baylin, S.B., 2017. CHD4 has oncogenic functions in initiating and maintaining epigenetic suppression of multiple tumor suppressor genes. Cancer Cell 31, 653–668.e7.
Xian, Y., Xiao, C., 2020. The structure of ASFV advances the fight against the disease. Trends Biochem. Sci. 45, 276–278.
Zhang, L., Misiara, L., Samaranayake, G.J., Sharma, N., Nguyen, D.M., Tahara, Y.K., Kool, E.T., Rai, P., 2021. OGG1 co-inhibition antagonizes the tumor-inhibitory effects of targeting MTH1. Redox Biol. 40, 101848.
Zhou, X., Li, N., Luo, Y., Liu, Y., Miao, F., Chen, T., Zhang, S., Cao, P., Li, X., Tian, K., Qiu, H.J., Hu, R., 2018. Emergence of African swine fever in China, 2018. Transbound Emerg Dis 65, 1482–1484.